Ultrasonically Regenerable Nano-Phase Change Emulsions with Low Supercooling and High Shear Stability

Yuyao Guo,[a] Jinxin Feng,[b] Zhihao Xia,[b] Ziye Ling,[*ab] Xiaoming Fang[ab] and Zhengguo Zhang[*ab]

[a]Key Laboratory of Enhanced Heat Transfer and Energy Conservation, The Ministry of Education, School of Chemistry and Chemical Engineering, South China University of Technology, Guangzhou, 510640, China

[b]Guangdong Engineering Technology Research Center of Efficient Heat Storage and Application, South China University of Technology, Guangzhou 510640, China

[*]Corresponding authors: zyling@scut.edu.cn (Z. L.); cezhang@scut.edu.cn (Z. Z.).

Nano-phase change emulsions (NPCEs) are attractive thermal fluids for applications such as cold-chain logistics, vaccine storage, and low-temperature energy systems operating in the 0–20 ℃ range. However, their deployment is hindered by significant supercooling and poor stability under shear. Here, we report a formulation strategy combining surfactant and nucleating agent optimization to prepare NPCEs with suppressed supercooling (<0.5 ℃) and high dispersion stability. The NPCEs maintain structural integrity after 24 h of continuous shear at 5 ℃, with droplet size variation within 20 nm. Rheological and microscopic analyses elucidate the interfacial disruption mechanism under low-temperature shear, and a nucleating agent selection principle is established based on molecular conformation and crystallization compatibility. To address performance degradation, we develop a high-energy ultrasonic on-line regeneration method that rapidly restores thermal functionality without system downtime. The NPCEs achieve >99.5% latent heat recovery and maintain stable performance over 60 days of thermal and mechanical cycling. This work demonstrates a regenerable NPCE system featuring ultra-low supercooling and long-term operational stability. The findings offer a practical pathway for scalable deployment of advanced thermal fluids in energy-efficient industrial applications.

Keywords: Nano-phase change emulsions; Low-temperature stability; Supercooling control; High-energy regeneration technique; Nucleating agent selection.

Industrial Chemistry & Materials Accepted Manuscript

1. Introduction

Phase change materials (PCMs) have attracted considerable attention in thermal energy storage (TES) systems due to their high energy density and reversible latent heat characteristics.[1] They have been widely used in cooling,[2] solar thermal utilization,[3] and industrial waste heat recovery applications.[4-6] In recent years, phase change emulsions (PCEs)—a novel class of storage media formed by dispersing micro- or nano-scale PCM droplets in a continuous fluid phase—have emerged as a promising alternative to traditional phase change slurries (PCSs).[7] Compared with hydrate slurries,[8] microcapsule-based emulsions,[9] and micro-emulsions,[10] PCEs offer advantages in ease of preparation, thermal resistance regulation, and storage capacity, paving the way for advanced thermal management solutions.[11]

In low-temperature (0–20 °C) thermal management fields such as cold chain logistics, biomedical refrigeration, and data center cooling, PCEs exhibit great potential due to their efficient heat storage and temperature regulation capabilities. However, their practical applications face two major challenges: droplet instability [12] and severe supercooling.[13] The former is primarily induced by shear disturbances, thermal cycling, and interfacial tension variation during operation,[14] leading to droplet flocculation, coalescence, or phase separation.[15] These effects result in increased particle size, reduced surface area, and degraded heat transfer efficiency.[16] The use of nano-phase change emulsion (NPCE) structures has been explored to leverage Brownian motion for enhanced dispersion stability.[17-19] Meanwhile, supercooling refers to the delayed crystallization of PCMs upon cooling, which significantly impairs the latent heat release and phase transition repeatability. Various nucleating agents, such as cellulose nano-fibers,[20] graphite particles,[21, 22] metal oxides,[23] long-chain alkanes[24-26] and alcohols,[27, 28] have been introduced to induce heterogeneous nucleation and reduce the supercooling degree. Cabaleiro et al.[29] employed three high-melting-point nucleating agents to reduce the supercooling degree of NPCEs from 13 °C to approximately 3 °C. Similarly, Zhang et al.[30] introduced nano-TiO$_2$, successfully lowering the supercooling degree from 21.7 °C to 5 °C. Although these studies demonstrated effective suppression

of supercooling, the incorporation of solid nanoparticles may adversely affect the long-term stability of the NPCEs.

In addition to structural factors, operational conditions such as low temperature and flow-induced shear further exacerbate emulsion degradation. Liu et al.[31] reported that after 70 days of circulation in a pipe heat exchanger, the supercooling degree of NPCEs increased from 2.8 ℃ to over 10 ℃, highlighting the long-term instability under dynamic conditions. Vilasau et al.[32] observed that under free-fall shear, droplet size increased from 1.0 μm to 6.7 μm, with significant flocculation and circuit blockage. However, the effects of shear rate, component ratio, and their coupling mechanisms remain poorly understood. Liu et al.[24] further showed that long-term pump-driven cycles led to latent heat decay and supercooling rebound, yet few studies have systematically analyzed degradation behavior under complex coupled conditions involving temperature fluctuation, thermal cycling, and shear flow. Moreover, existing strategies for performance recovery—mainly low-energy re-dispersion[31]—are inefficient and require system shutdown, which is impractical for continuous operation.

To address the dual challenges of supercooling control and structural instability in NPCEs under low-temperature conditions, this study investigates the following:

1. A surfactant–nucleating agent co-optimization strategy to develop NPCEs with high dispersion stability and ultra-low supercooling (<0.5 ℃);

2. A comprehensive evaluation of emulsion degradation mechanisms covering static storage, thermal cycling, isothermal shear, and flow heat exchange, with a molecular-level analysis of nucleating agent structure–performance relationships;

3. A high-energy regeneration method to enable rapid recovery of emulsion performance (>99.5% enthalpy recovery) while maintaining continuous system operation.

The findings provide a mechanistic understanding of NPCE degradation under real-time operation and offer practical solutions for long-term reliability in cold chain and low-temperature energy systems.

2. Results and discussion

2.1 Enhancement of static stability and supercooling suppression

To develop high-performance NPCEs with low supercooling, excellent static stability, and favorable thermal–flow properties, a formulation strategy was adopted based on the synergistic optimization of surfactant type, concentration, and nucleating agent dosage. A comprehensive evaluation was conducted on the thermal behavior, droplet size distribution, and viscosity of various formulations under both static storage and thermal cycling conditions. For low-temperature applications, a composite phase change material (PCM) was formulated by blending pentadecane and hexadecane in a 1:1 mass ratio, resulting in a melting temperature of approximately 10 ℃. The key thermophysical properties of the composite PCM are summarized in Table S2, including a latent heat of 195.1 kJ kg^{-1}, specific heat capacity of 2.0 kJ kg^{-1} ℃$^{-1}$, dynamic viscosity of 5.2 cP, and density of 771.0 kg m^{-3}.

As shown in Fig. S3a-S3d, a mixture of Tween 60 and Span 60 (T60-S60) exhibited excellent performance among the six surfactants tested. NPCEs prepared with T60–S60 (HLB = 8) achieved an average droplet size below 200 nm, low viscosity (~2 cP at 100 s^{-1}), and maintained a supercooling degree under 1 ℃ after 50 thermal cycles. Differential Scanning Calorimetry (DSC) indicated dual freezing peaks, suggesting enhanced heterogeneous nucleation due to a well-structured hydrophilic–hydrophobic interface. Tuning the HLB value further confirmed that HLB = 8 offers an optimal balance between dispersion stability and crystallization behavior, as shown in Fig. S4a-S4d. Higher HLBs reduced droplet size but led to decreased freezing temperatures and narrower peaks, indicating deteriorated nucleation activity. As shown in Fig. S5a-S5d, the surfactant-to-oil (S/O) ratio was also critical: increasing S/O from 1:10 to 1:2 reduced droplet size but raised viscosity significantly. At S/O = 1:5, the system achieved a desirable compromise—small droplet size (<200 nm), low viscosity (2 cP), and negligible supercooling. Tetradecanol (C14-OH) was selected as the nucleating agent, with an optimal dosage of 2wt%. At this concentration, supercooling dropped to below 0.5 ℃, as shown in Fig. S6a-S6d, while the emulsion maintained good stability

and low viscosity. Excessive addition (>2wt%) led to droplet coarsening and phase separation after cycling, as shown in Fig. S7a-S7c.

Based on the systematic evaluation of different surfactant systems, HLB values, S/O ratios, and nucleating agent concentrations (as shown in Table S1), the formulation consisting of T60–S60 (HLB = 8), 2wt% C14-OH, and an S/O ratio of 1:5 was identified as the optimal formulation. Using this optimized formulation, NPCEs containing 10 and 20wt% PCM achieved latent heats of 14.10–29.72 J g^{-1} while maintaining droplet sizes below 300 nm and supercooling degrees under 0.5 ℃ after 300 thermal cycles. As shown in Figs. 1c and 1d, the particle size distributions of 10 wt% and 20 wt% emulsions remained monomodal and narrow, with no secondary peaks. Droplet sizes increased moderately from 210 ± 3 nm and 224 ± 1 nm to 282 ± 1 nm and 296 ± 11 nm after 300 thermal cycles, representing less than 30% change. Zeta potentials remained above 40 mV with less than 10% variation (Fig. S13), indicating no obvious aggregation or phase separation. These results demonstrate excellent static stability and thermal responsiveness, highlighting the potential of the developed NPCEs for reliable low-temperature thermal storage.
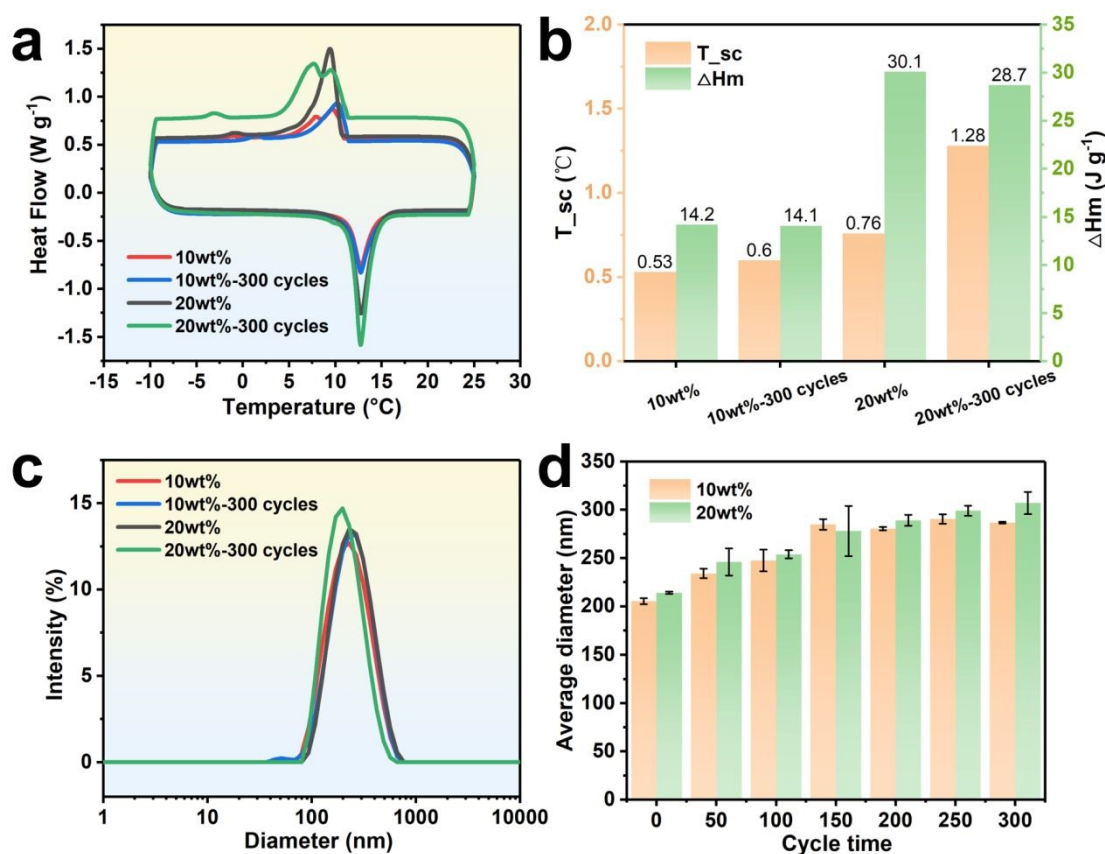
Fig. 1 (a) DSC curves; (b) supercooling and enthalpy; (c) droplet size distributions; (d) variation of droplet size with cycle number for NPCEs with different PCM contents.

2.2 Influence of core components on the stability of NPCEs under low-temperature dynamic shear

2.2.1   Destabilizing effects of low-temperature dynamic shear on NPCEs

Although NPCEs exhibit good stability under static conditions, their structural integrity significantly deteriorates under dynamic shear conditions such as continuous stirring and flow at low temperatures (5 ℃).

One of the primary contributing factors is the drastic change in viscosity during cooling. As the temperature decreased from 25 ℃ to 5 ℃, the viscosity of the emulsion increased sharply from 7 cP to 4862 cP. This rheological shift was accompanied by a corresponding increase in average droplet size from 193 nm to 618 nm, along with a reduction in absolute zeta potential from 49.35 mV to 42 mV (Fig. 2a and 2b). Extended stirring under these conditions led to visible bulk morphological changes. The emulsion expanded in volume by approximately 20% and formed a foam-like structure resembling "whipped cream" (Fig. 2c). Notably, this structure did not recover upon cessation of shear, and strong coalescence tendencies were observed.

These results clearly demonstrate that the combined effects of low temperature and mechanical shear significantly compromise the colloidal stability of NPCEs, manifesting in droplet growth, reduced electrostatic repulsion, and irreversible structural deformation.
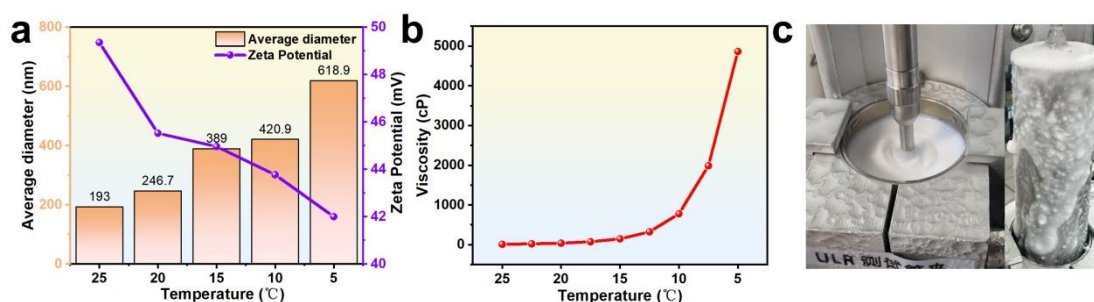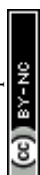

Fig. 2 (a) Droplet size and zeta potential variation during cooling; (b) viscosity changes; (c) photograph of viscometer rotor after shearing at 5 ℃ for 1 h for NPCEs with tetradecanol nucleating agent.

2.2.2 Intrinsic instability of NPCEs at low temperatures

To elucidate the mechanisms of emulsion destabilization at low temperatures, this section investigates the evolution of physical properties using NPCEs without nucleating agents (No NA) as a simplified reference. Droplet size, viscosity, and microstructure were monitored under continuous shear at different temperatures.

At ambient temperature (25 ℃), NPCEs exhibited excellent stability. As shown in Fig. 3a-c, after 15 days of shear, the average droplet size remained near 200 nm with negligible increase, the zeta potential remained above 45 mV and the latent heat decreased by only 1.8%, indicating strong electrostatic repulsion and robust colloidal stability. Zeta potentials above 30 mV are generally considered indicative of stable dispersions, while values exceeding 40 mV reflect colloidal stability.[7] Microscopy (Fig. S8a) confirmed uniform dispersion and intact structure. In contrast, significant degradation occurred under shear at 5 ℃. Despite minor changes in latent heat and supercooling (Fig. 3e), viscosity increased from 3.31 to 4.33 cP , droplet size grew from 187.6 to 308.7 nm and zeta potential dropped below 40 mV (Fig. 3d, 3f), indicating coalescence. Microscopy (Fig. S8b) showed larger droplets after 15 days.

Given that water remains largely unchanged between 5–25 ℃, these effects likely stem from PCM and surfactant transitions. The PCM solidifies at 5 ℃ (freezing point ~10 ℃), increasing friction and viscosity during shear. Meanwhile, DSC results (Fig. S9) show that Tween 60 and Span 60 melt at 21.8 ℃ and 51.5 ℃, respectively, implying partial surfactant solidification at 5 ℃. The DSC analysis confirms that both the PCM and surfactant solidify at this temperature. Combined with interfacial behavior analysis, the low temperature and phase transition reduce the surfactant coating efficiency, as reflected in decreased adsorption, reduced micelle formation, and weakened interfacial film strength[33]. Under these conditions, shear is more likely to cause droplet adhesion, leading to increased particle size and reduced stability. This may reduce interfacial activity and film strength, promoting droplet coalescence (Fig. 3g).These observations align with Gibbs free energy-driven aggregation[34]: elevated viscosity restricts droplet mobility, favoring coalescence to minimize interfacial

energy. Insufficient interfacial flexibility further accelerates droplet bridging and growth.

However, no significant creaming or phase separation was observed in No NA NPCEs, indicating that surfactant solidification alone is not the primary cause of instability. The next section explores the role of nucleating agents in enhancing NPCE stability under such conditions.
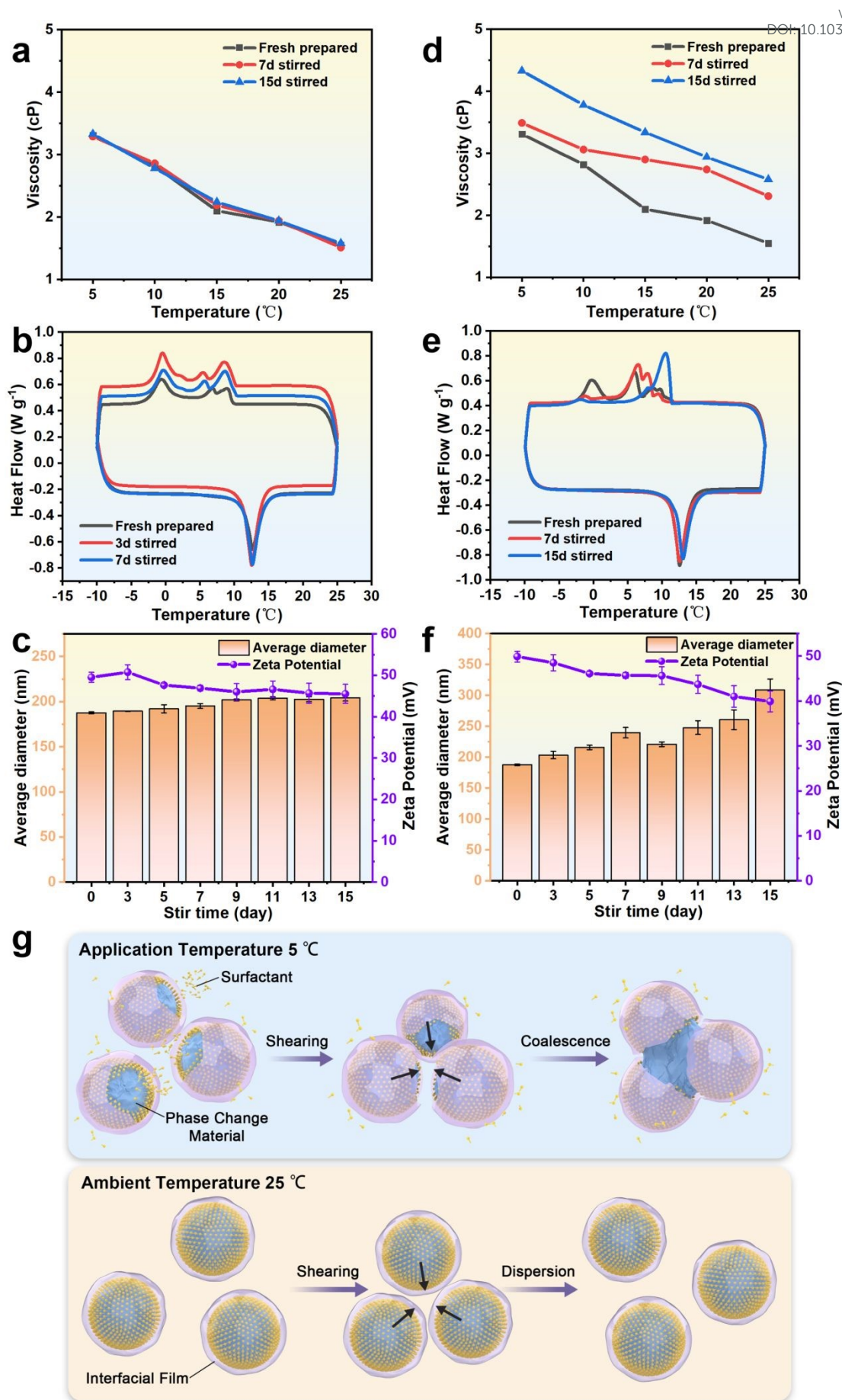
Fig. 3 Comparison of (a) viscosity (b) DSC (c) particle size and zeta potential of NPCEs stirred at 25 °C for 15 days; (d) viscosity, (e) DSC, (f) particle size and zeta potential of NPCEs stirred at 5 °C for 15 days; (g) schematic representation of the aggregation mechanism of NPCEs at low temperatures.

2.2.3 Effect of nucleating agents on the dynamic stability of NPCEs at low temperature

To assess the influence of nucleating agents on emulsion stability, four aliphatic alcohols—tetradecanol (C14-OH), hexadecanol (C16-OH), octadecanol (C18-OH), and octacosanol (C28-OH)—were tested under shear at 5 °C. Structural changes and stability degradation were analyzed.

After 30 minutes of low-temperature shear, NPCEs with C14-OH, C16-OH, and C18-OH showed clear signs of creaming and coalescence, including phase separation and rotor adhesion (Fig. 4a), with a sharp loss in fluidity. Droplet sizes increased significantly—by 426 nm, 1059 nm, and 3277 nm, respectively—far exceeding the 121.1 nm increase in the no-NA control (Fig. 4d).C18-OH led to the most severe instability: viscosity rose from 26 cP at 25 °C to 8891 cP at 5 °C, and the emulsion became non-flowable even under mild agitation at 15 °C (Fig. 4c, 4e and 4f). Cryo-TEM images (Fig. 4f) confirmed interfacial breakdown and droplet coalescence. In contrast, the C28-OH emulsion remained stable, showing minimal changes in droplet size and viscosity. Remarkably, even after 10 hours of shearing, the zeta potential changed by less than 5%, indicating that the electrostatic stability was maintained. However, its supercooling reduction was limited, suggesting the polar hydroxyl group may hinder crystallization control.

To decouple polarity effects, nonpolar alkane-based nucleating agents—tetradecane (C14), eicosane (C20), octacosane (C28), and hexatriacontane (C36)—were tested. As shown in Fig. 4g and 4h, all alkane-based NPCEs exhibited excellent low-temperature shear stability (droplet size increase <12%) and effective supercooling suppression. Among them, C28 stood out: after 10 h of shear, droplet size remained ~219 nm with PDI < 0.2 and supercooling nearly eliminated. After 24 h of shear, the C28 emulsion maintained over 95% size distribution consistency (Fig. 4i) and a uniform spherical morphology without aggregation (Fig. S10a and S10b).

These results demonstrate that combining C28 with Span 60 and Tween 60 constitutes an effective surfactant–nucleating agent co-optimization strategy, enabling the fabrication of high-performance NPCEs with both minimal supercooling and outstanding low-temperature shear stability. Owing to its superior stability, nucleation efficiency, and droplet size control, C28 was selected as the representative alkane-based nucleating agent for further comparison with alcohol-based systems. This synergistic approach is critical for maintaining structural integrity and thermal reliability during long-term operation in low-temperature thermal management applications.
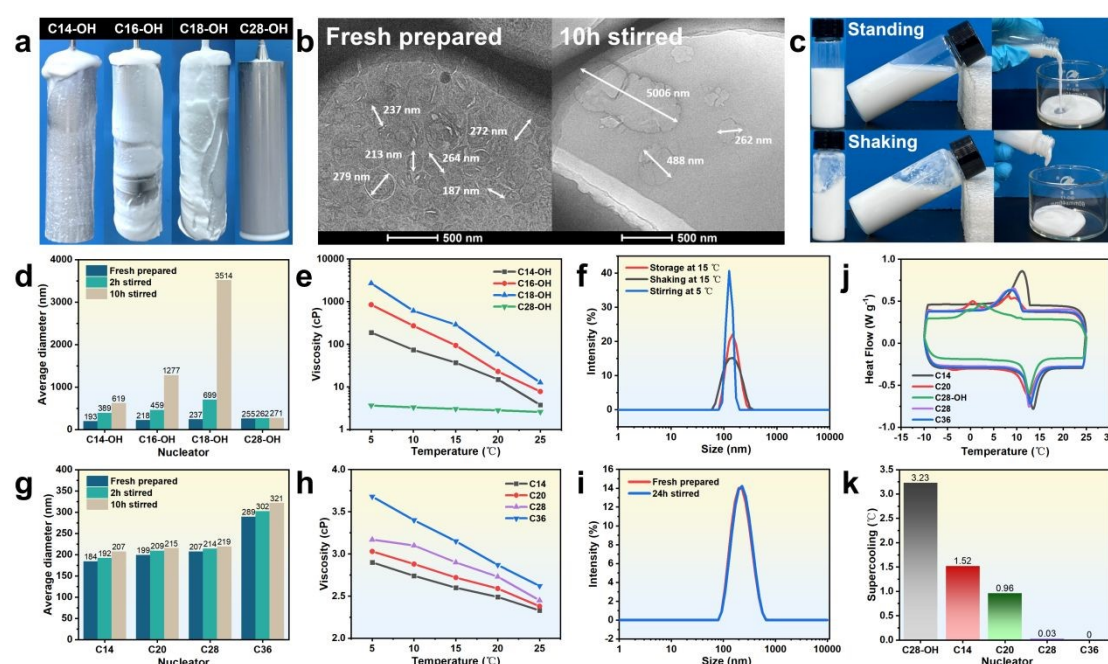

Fig. 4 (a) Photographs of the viscometer rotor of NPCEs with alcohol nucleating agents after stirring at 5 ℃ for 30 min; (b) Cryo-TEM images of C18-OH NPCEs before and after stirring at 5 ℃ for 30 min; (c) Flow characteristics of C18-OH NPCEs before and after oscillation at 15 ℃; (d) Viscosity and (e) droplet size variations of NPCEs with alkane nucleating agents at 5 ℃; (f) Particle size distribution of C18-OH NPCEs under different conditions; (g) Droplet size and (h) viscosity changes of NPCEs with alkane nucleating agents at 5 ℃; (i) Particle size distribution of C28 NPCEs before and after shearing at 5 ℃ for 24 h; (j) DSC curves and (k) supercooling of NPCEs with different nucleating agents.

2.2.4 Mechanistic analysis of the dynamic stability of NPCEs at low temperature

This section explores how different nucleating agents influence the dynamic stability of NPCEs under low-temperature shear. Experimental results show that short-chain alcohol-based nucleating agents (e.g., C18-OH) significantly reduce

interfacial tension and enhance repulsive forces at the droplet interface, leading to excellent dispersion under static conditions. However, under low-temperature shear, exhibit poor stability under shear. In contrast, long-chain nucleating agents such as C28-OH and C28 demonstrate much greater structural integrity under the same conditions. To elucidate the microscopic mechanism of interfacial film destabilization, we investigated the interfacial structural evolution as influenced by the molecular configurations of nucleating agents, supported by microscopy, zeta potential, and interfacial tension data.

Negative-stain microscopy and cryo-TEM imaging (Fig. 5a, 5b, 5c and 5d) reveal that C18-OH-stabilized NPCEs exhibit sharp interfacial boundaries and strong static dispersion, suggesting a dense and ordered interfacial film. In cryo-TEM images, C18-OH droplets appear shriveled with bright rims, indicating a brittle interfacial film vulnerable to shear-induced fracture. In contrast, droplets stabilized by C28-OH and C28 exhibit smoother contours and more diffuse boundaries, indicative of more flexible and resilient interfacial structures. This flexibility enhances shear resistance and maintains structural integrity at low temperatures.

Interfacial property measurements further support the above observations. As shown in Fig. 5e, 5f and 5g, C14-OH and C18-OH significantly reduced the surface tension of the emulsion system by 26% and 54%, respectively. The zeta potential of the C18-OH system exceeded 50 mV, reflecting a strong enrichment of polar groups at the droplet interface. Additionally, the storage modulus of the C18-OH emulsion was found to be 39 times that of C28 and 840 times that of the emulsion without nucleating agents, indicating a densely packed, rigid interfacial film. This rigidity arises from the chain-length compatibility between C18-OH and the surfactants Span 60/Tween 60, which enables cooperative packing and densification of the interfacial membrane.

Nevertheless, such tightly packed interfacial structures can become stress-concentration zones under low-temperature shear. As the surfactants tend to solidify at low temperatures, the interfacial film becomes even more rigid, promoting stress accumulation along crystal boundaries. This leads to interface rupture and droplet

aggregation, resulting in a sharp increase in droplet size and severe loss of emulsion stability. Consequently, the C18-OH emulsion exhibited a dramatic 1380% increase in average droplet size after shear, indicating the least dynamic stability among all tested samples. C14-OH, which also contains polar hydroxyl groups, can participate in interfacial film formation. However, due to its shorter carbon chain compared to Span 60/Tween 60, its incorporation leads to a less compact interfacial structure. As shown in Fig. 5b, C14-OH-stabilized droplets also exhibit a faint white rim, but with a thinner, less wrinkled interfacial layer, suggesting lower film rigidity. The reduction in surface tension and zeta potential was also less significant than in the C18-OH case. As a result, the increase in droplet size after shear was limited to 221%, with a lower degree of degradation. In contrast, although C28-OH contains a hydroxyl group, its longer carbon chain makes it less capable of co-assembling with surfactants to form a compact interfacial film. Consequently, it lacks interfacial densification and shows shear stability similar to that of nonpolar C28. This indicates that C28-OH also provides excellent stability under dynamic shear conditions.

Fig. 5h illustrates the schematic evolution of droplet interfacial structures under low-temperature shear for various nucleating agents. In C18-OH systems, chain-length compatibility with Span 60/Tween 60 facilitates tight interfacial packing at the droplet interface. This results in a rigid interfacial film with limited flexibility, which is prone to microcrack formation under shear stress. Crystallization and volume expansion during the phase change aggravate film degradation, triggering coalescence and destabilization. In comparison, the shorter chain of C14-OH exhibits weaker compatibility with the surfactants, resulting in a looser and less rigid interfacial structure. While some aggregation occurs under shear, structural damage is moderate due to lower stress concentration at the interface. For C28 and C28-OH, the long hydrocarbon chains are sterically hindered from integrating into the interfacial layer and instead form segregated hydrophobic domains. This preserves interfacial flexibility and prevents shear-induced rupture, thereby significantly enhancing dynamic stability.
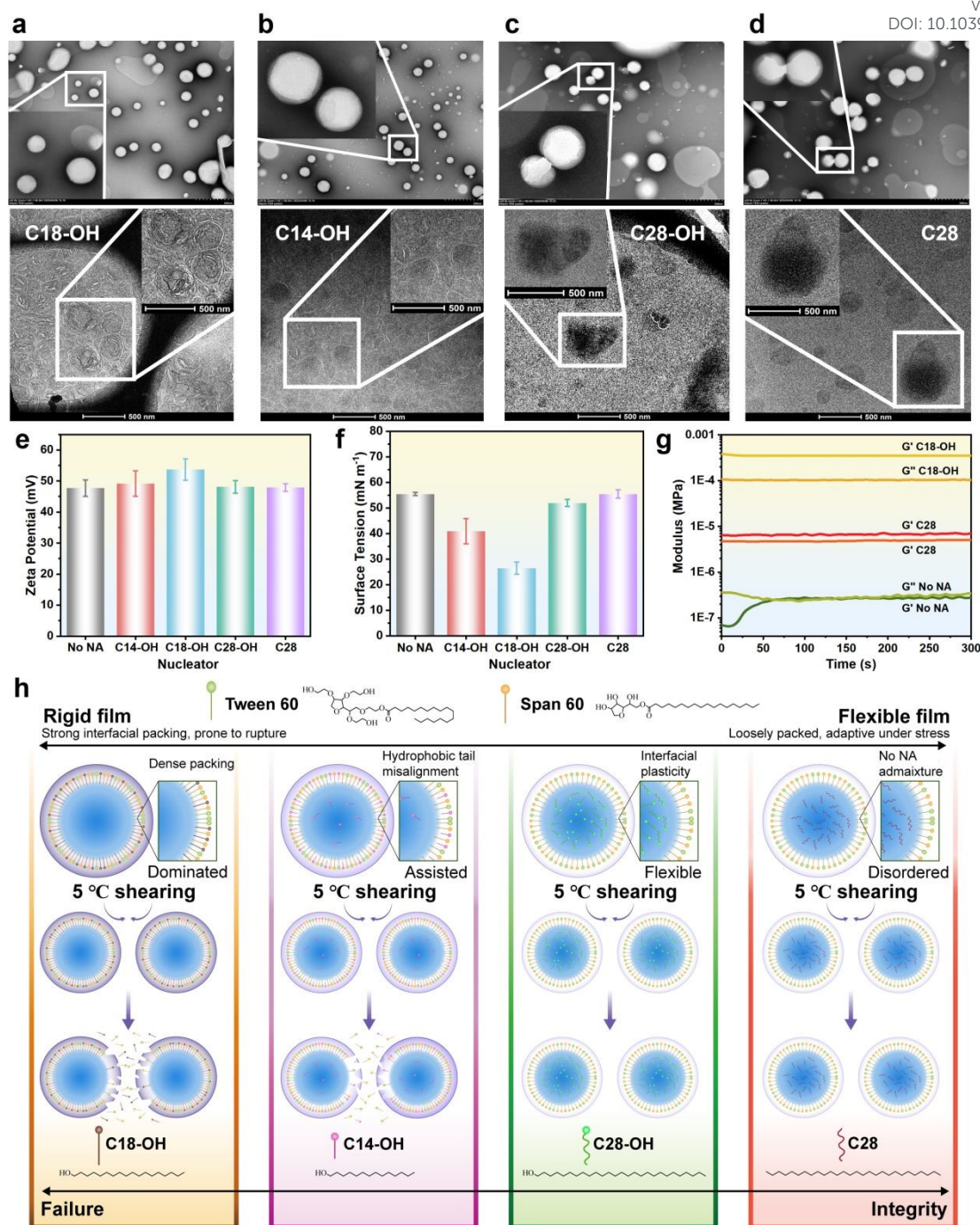
Fig. 5 Negative staining microscopy images of NPCEs with different nucleating agents: (a) C18-OH, (b) C14-OH, (c) C28-OH, and (d) C28; Cryo-TEM images: (e) C18-OH, (f) C14-OH, (g) C28-OH, and (h) C28; comparison of (f) zeta potential, (g) surface tension, and (e) modulus of different nucleating agent NPCEs; (h) Schematic diagram of the mechanism underlying the difference in low-temperature stability of NPCEs with different nucleating agents.

As shown in Fig. S11a and S11b, Raman spectroscopy and ¹H-NMR analyses revealed no chemical bond differences between C28 and C28-OH, indicating that their contrasting nucleation behaviors result from differences in molecular distribution rather than composition. The polar hydroxyl group in C28-OH tends to localize at the

droplet interface, limiting its ability to penetrate the hydrophobic PCM core and causing polar repulsion with paraffin. This weakens its nucleation efficiency and increases supercooling relative to the nonpolar C28.

Overall, NPCE instability under low-temperature shear is primarily due to rigid interfacial film rupture. Nucleating agent behavior can be summarized as follows:

- Polar nucleating agents, especially those with chain lengths matching surfactants (e.g., C18-OH), enhance interfacial compactness and static stability but lead to film rigidity and shear-induced failure.

- Molecular polarity and conformation affect the trade-off between nucleation and flexibility. C14-OH initiates nucleation but suffers from limited stability due to rigid interfacial structure. C28-OH, though more flexible, shows weak nucleation due to its limited penetration and residual polarity.

- Nonpolar long-chain agents like C28 avoid interfacial disruption and effectively promote nucleation within the PCM core, offering both thermal and mechanical stability.

Based on these findings, two design principles for nucleating agents are proposed:(1) Avoid surfactant-length matching to preserve interfacial flexibility and prevent rupture;(2) Favor nonpolar long-chain molecules that enhance nucleation while maintaining structural integrity.

These findings establish a molecular-level rationale for the surfactant–nucleating agent co-optimization strategy, highlighting the exceptional compatibility between C28 and Span 60/Tween 60 in achieving both minimal supercooling and outstanding low-temperature shear stability. Based on this optimization, C28 has been selected as the representative nucleating agent for subsequent investigations on NPCE performance under continuous-flow heat exchange conditions.

2.3 Investigation of long-term continuous flow heat transfer and regeneration performance of NPCEs

Building upon the previous constant-temperature heat transfer experiments, this section introduces a simulated in-pipe flow heat transfer process to assess the stability
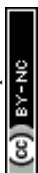
and thermal performance of NPCEs under dual perturbations: cyclic melting–solidification and flow-induced shear, simulating real-world application conditions. To address performance degradation during long-term operation, an online high-energy regeneration technique is also designed and validated, enabling real-time restoration of emulsion performance within the heat exchange system.

2.3.1 Stability characteristics of NPCEs during continuous flow heat transfer

To replicate practical engineering conditions, a 10-liter-scale closed-loop heat transfer system was constructed with inlet and outlet temperatures both set at 20 ℃. By adjusting the flow and heat exchange conditions, the outlet temperature was maintained at a constant 5 ℃, ensuring that the NPCEs underwent full melting–solidification cycles during circulation (as illustrated in Fig. S12).

Comparison of emulsion stability under static and continuous flow conditions revealed that shear forces significantly exacerbated emulsion destabilization. As shown in Fig. 6a, the NPCEs maintained excellent storage stability over 90 days of static storage, with droplet size variation below 5%, zeta potential consistently above 45 mV, and viscosity stable at approximately 2.3 cP. However, under continuous flow heat exchange for just 30 days, droplet sizes increased beyond 700 nm, zeta potential dropped below 35 mV, and viscosity rose to 4.5 cP (Fig. 6b and 6c). Polarized optical microscopy (Fig. 6d) further revealed pronounced droplet aggregation, reduced inter-droplet spacing, and clear signs of shear-induced coalescence, indicating significant damage to the interfacial stabilization structure caused by continuous shear stress. These results emphasize the crucial influence of flow-induced mechanical stresses on the long-term stability of NPCEs and the necessity for regeneration strategies to maintain functional performance under realistic operational conditions. While the NPCEs showed excellent performance under moderate conditions, partial freezing and increased viscosity were observed near −5 ℃ in low-flow regions, indicating room for further enhancement in extreme environments. Future work will explore modifications to the base fluid composition to improve antifreeze properties and broaden the operational temperature range of the emulsions.

As shown in the DSC curves in Fig. 6e and 6f, despite the observed changes in droplet size, viscosity, and flow behavior, the thermal properties of the NPCEs remained largely unaffected. After 30 days of continuous flow heat exchange, the phase change temperature exhibited negligible drift, and the degree of supercooling remained below 0.2 ℃, indicating that the system retained good thermal reversibility and phase transition stability. The latent heat of phase change decreased by 5.13 J g^{-1}, suggesting a slight reduction in effective heat storage capacity, likely due to partial droplet coalescence and emulsion breakdown.
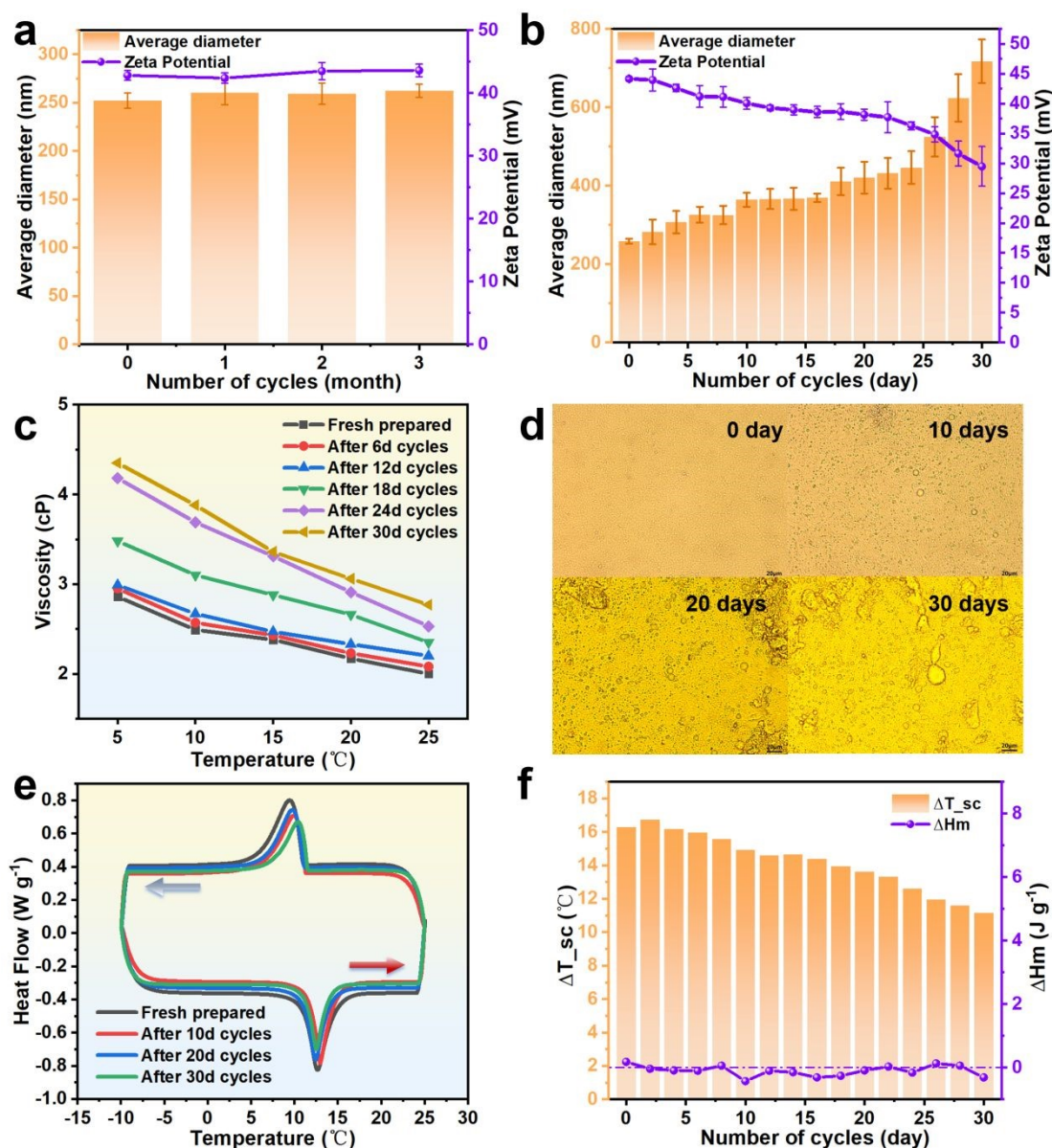

Fig. 6 (a) Droplet size and (b) zeta potential as a function of time at rest and under flow; (c) viscosity variation; (d) polarization microscopy images; (e) DSC curves; (f) enthalpy and supercooling evolution of NPCEs under different flow-based heat transfer durations.

Industrial Chemistry & Materials

2.3.2 Regeneration performance study of NPCEs

To address the significant increase in droplet size and the associated decline in emulsion stability, a high-energy ultrasonic regeneration strategy was developed and implemented. As illustrated in Fig. 7, after 30 days of continuous operation, NPCEs showed increased droplet size and viscosity due to prolonged low-temperature shear. To restore performance without interrupting circulation, an online ultrasonic regeneration strategy was applied. An ultrasonic disruptor was inserted into the storage tank and operated at three fixed depths (surface, 5 cm, and 10 cm) for 10 minutes each (50% power, pulsed 2 s on / 2 s off), while the emulsion continued flowing through the heat exchanger. Regeneration was achieved through acoustic cavitation and interfacial disruption, which broke up large droplets and facilitated surfactant re-adsorption, thereby recovering uniform droplet size and emulsion stability (Fig. 7 30d data). During this process, the NPCE continued to flow through the heat exchange system under preset temperature and flow conditions. Therefore, this approach effectively restores emulsion performance in real time while maintaining structural integrity and uninterrupted thermal–flow stability during continuous operation.
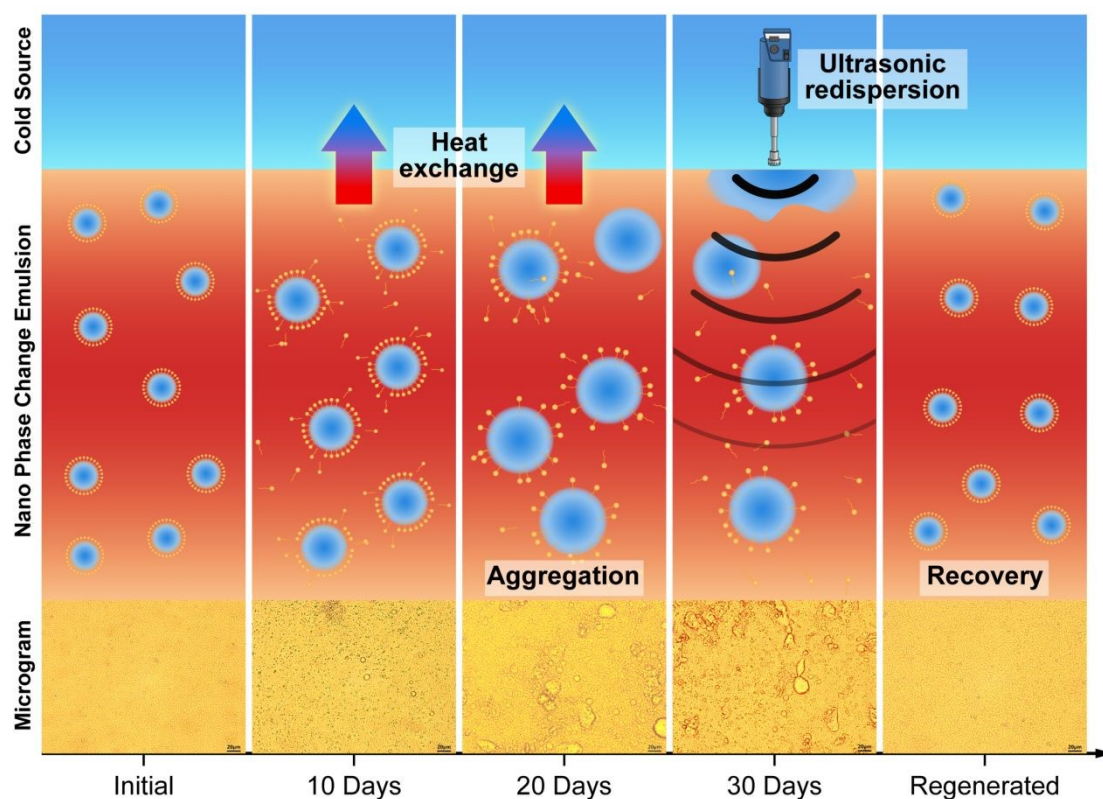
Industrial Chemistry & Materials Accepted Manuscript

Fig. 7 Schematic diagram of NPCE regeneration during flow-based heat exchange.

Experimental results demonstrate that the proposed high-energy regeneration method effectively restores the performance of NPCEs degraded by prolonged flow and thermal cycling. As shown in Fig. 8a, the droplet size distribution after regeneration closely matches that of the freshly prepared emulsion, indicating a successful recovery of the initial microstructure. Furthermore, Fig. 8b shows that the regenerated emulsion exhibits a similar droplet growth trend over the next 30 days of flow heat exchange as the original emulsion, confirming that the coalescence tendency has been effectively suppressed. In terms of thermal performance, Fig. 8c shows that the phase change enthalpy of the regenerated emulsion is restored to its initial value, with a variation of less than 0.5%. This recovery is further supported by the DSC curve in Fig. 8e, which clearly indicates the enthalpy rebound, verifying that the regeneration process successfully restores latent heat capacity. Viscosity measurements in Fig. 20d reveal a reduction from 4.3 cP to 2.9 cP after regeneration, approaching the initial value of 2.8 cP, reflecting a marked improvement in emulsion flowability. Regarding heat transfer capability, Fig. 8f shows that after extended use, the emulsion exhibited a 21.6% decline in average cooling power due to demulsification and reduced phase change enthalpy. Following regeneration, however, the thermal properties of the emulsion were restored, enabling the average heat exchange power to recover to 98% of its original level, with nearly identical power curves before degradation and after regeneration.

Results from a 60-day study involving two regeneration cycles further confirm the effectiveness of the strategy. Without regeneration, the emulsion showed an average droplet size increase of over 100%, a 33% decrease in Zeta potential, a ~54% increase in viscosity, and a 17% reduction in phase change enthalpy after every 30 days of flow heat exchange. In contrast, after each regeneration, the droplet size deviation was controlled within ±10%, viscosity was restored within ±5% of the original value, and the phase change enthalpy variation remained below ±0.5%, with up to 98% recovery in thermal power. These results robustly validate the proposed high-energy regeneration strategy, demonstrating its effectiveness in restoring microstructure, physicochemical properties, and system-level heat transfer capacity. This provides a

critical foundation for the long-term, stable operation of NPCE-based thermal energy

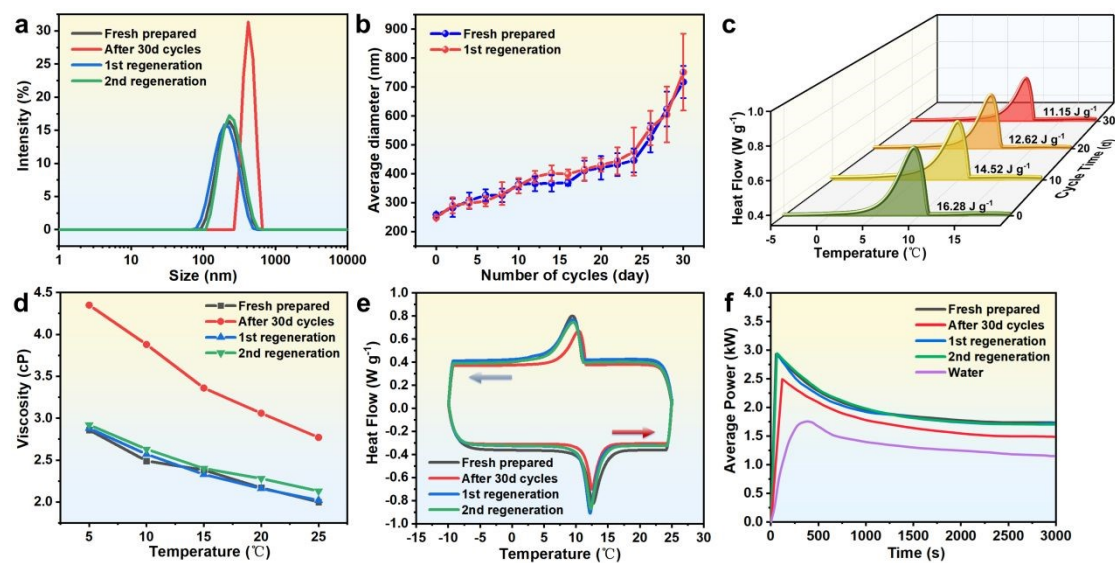storage systems in practical engineering applications.

Fig. 8 (a) Droplet size distributions before and after regeneration; (b) variation of droplet size with cycle number; (c) enthalpy; (d) viscosity; (e) DSC curves; (f) average instantaneous cooling power in the flow-based heat exchange system.

3. Conclusions

This study addresses the dynamic instability of NPCEs under low-temperature conditions by integrating interfacial regulation, nucleating agent design, and online regeneration. The main findings are:

1. Interfacial instability mechanism: Continuous flow heat exchange for 30 days led to a 178% increase in droplet size and a viscosity rise to 4.4 cP, confirming that shear stress is a key factor in emulsion degradation.

2. Structure–interface correlation: C28, a nonpolar long-chain alkane, effectively induces nucleation (supercooling < 0.2 ℃) while maintaining interfacial flexibility, enabling both low supercooling and dynamic stability.

3. Nucleating agent design principles:(i) Avoid carbon chain lengths that exactly match the surfactant to preserve interface flexibility;(ii) Prefer nonpolar molecules to prevent interfacial interference.

4. Online regeneration strategy: A high-energy ultrasonic method restored NPCE properties within 30 minutes, achieving near-complete recovery in droplet size, viscosity, and latent heat. This enables real-time restoration during operation.

Overall, the study introduces dynamic stability as a critical performance metric for NPCEs and bridges microstructural design with macroscopic performance. The proposed strategies offer a pathway for the long-term, stable application of NPCEs in thermal energy storage systems. These findings provide practical guidance for employing NPCEs as working fluids in low-temperature heat transfer systems, where integrated ultrasonic regeneration enables real-time performance recovery without disrupting circulation, supporting continuous operation in applications such as electronics cooling, building HVAC, and renewable energy storage.

4. Experimental section

4.1 Preparation of low-temperature nano-phase change emulsions

4.1.1 Materials

Pentadecane (C15, purity 98.0%) and hexadecane (C16, purity 98.0%) were selected as the phase change materials, both obtained from Shanghai Macklin Biochemical Co., Ltd. Nonionic surfactants included Span 60, Tween 60, Brij 30, Triton X-100, and P123, all sourced from the same supplier. Ionic surfactants— sodium dodecyl sulfate (SDS, purity 99.9%) and cetyltrimethylammonium bromide (CTAB, purity 99.0%)—were provided by Tianjin Fuchen Chemical Reagent Co., Ltd.

The nucleating agents used included tetradecanol (purity 99.0%), hexadecanol (98.0%), octadecanol (98.0%), and octacosanol (96.0%), purchased from Shandong Yousuo Chemical Technology Co., Ltd. Additional alkane-based nucleating agents— tetradecane (98.0%), eicosane (98.0%), octacosane (98.0%), and hexatriacontane (96.0%)—were obtained from Shanghai Macklin Biochemical Co., Ltd. All chemicals were used as received without further purification. The selected fatty alcohols and alkanes were structurally similar to the main PCM components (pentadecane and hexadecane), allowing for high miscibility and molecular compatibility. This similarity enhances their ability to act as effective nucleating agents by promoting ordered crystallization within the dispersed phase. The properties of all selected nucleating agents are summarized in Table S3.

4.1.2 Preparation of NPCEs

In this study, a paraffin-based PCM composed of a 1:1 mass ratio of pentadecane and hexadecane was used to achieve a target phase change temperature of approximately 10 ℃. The NPCEs were prepared via ultrasonic emulsification [35], as illustrated in Fig. S1, using a PCM mass fraction of 10wt% and 20wt%.

First, the surfactant and nucleating agent were heated until liquefied and added to the base fluid (deionized water), followed by stirring at 85 ℃ and 200 rpm for 20

minutes to form a micellar dispersion. Next, the PCM was added to the aqueous phase

at a predetermined concentration and thoroughly mixed. The resulting mixture was

then transferred to an ultrasonic cell disruptor, operated at 50% power output (500 W)

with a 2 s on / 2 s off pulsed mode, and sonicated for 20 minutes to obtain a stable

nano-phase change emulsion.

The study first examined the effects of different types of surfactants on the

performance of the pentadecane–hexadecane NPCEs. Both ionic surfactants (SDS and

CTAB) and nonionic surfactants (Brij 30, P123, Tween 60–Span 60 (T60–S60), and

Triton X-100 (TX-100)) were evaluated. In addition, the influence of the hydrophilic-

lipophilic balance (HLB) of surfactants and the mass ratio of PCM to surfactant (S/O

ratio) on emulsion stability and performance were investigated.

Subsequently, the effect of nucleating agent content on the thermal and structural

behavior of the NPCEs was assessed. Finally, a comparative study was conducted to

evaluate the influence of alcohol-based and alkane-based nucleating agents on the

low-temperature dynamic stability of the NPCEs. Based on these tests, the optimal

formulation was determined, as summarized in Table S1.

Using the optimized formulation and component concentrations, approximately

10 L of NPCE was prepared for low-temperature application. The NPCEs were then

subjected to 60 days of flow heat exchange testing to monitor changes in supercooling

degree, droplet size, and thermal properties over time. These observations were used

to evaluate the long-term performance stability and degradation characteristics of the

prepared NPCEs.

4.1.3 Characterization of NPCEs

The average droplet size and polydispersity index (PDI) of the NPCEs were

measured using dynamic light scattering (DLS; Malvern Zetasizer Nano ZS). Each

sample was diluted 200 times and analyzed at 25 ℃ with a 120-second measurement

time, repeated three times. The measurement accuracy was within ±1%.

Surface tension was measured using a Dataphysics OCA 50 contact angle

analyzer, with each sample tested three times to obtain an average value. A ZEISS

MERLIN Compact field emission scanning electron microscope (FE-SEM) was used to observe the microstructure of freeze-dried NPCEs. Optical morphology was analyzed using a polarized optical microscope (POM, OLYMPUS GX71). Samples were diluted 20-fold with distilled water and observed at 500× magnification.

For transmission electron microscopy (TEM), NPCEs were negatively stained using a Hitachi HT-7800 microscope. A drop of emulsion was deposited onto a copper grid, stained with phosphotungstic acid, dried, and imaged at 100 kV. Cryo-TEM was conducted using an FEI Talos F200C operating at 200 kV. Samples were diluted 500-fold, deposited on 200-mesh EM grids, rapidly cooled in liquid nitrogen, and imaged to capture the nano-droplet morphology under liquid-phase conditions [36].

Viscosity was measured using a T-series viscometer (Shanghai Fangrui Instruments) in two modes. First, at room temperature, the shear rate was ramped from 1 to 100 s⁻¹ to determine the shear dependence of viscosity. Measurements were repeated three times within ±1% error. Second, temperature-dependent viscosity was tested under a fixed shear rate of 100 s⁻¹ using an external constant-temperature bath at 25 °C, 20 °C, 15 °C, 10 °C, and 5 °C.

Dynamic viscoelastic properties, including storage modulus (G') and loss modulus (G''), were measured using a TA Instruments ARES-G2 rheometer with a 60 mm diameter aluminum parallel-plate geometry and a 2 mm gap. Tests were conducted at 25 °C, with a 0.5% strain amplitude and 1 Hz oscillation frequency over 300 seconds. Each sample was tested three times and averaged, with a final measurement error below ±1%.

The phase change behavior and apparent specific heat of the NPCEs were evaluated using a differential scanning calorimeter (DSC, Q20, TA Instruments) under a nitrogen atmosphere at a flow rate of 50 mL·min⁻¹. Supercooling (ΔT) was calculated based on the temperature difference between melting point (T_m) and freezing point (T_f). The test accuracy was within ±1%, and the heating/cooling rate was 5 °C·min⁻¹.

The apparent thermal conductivity was measured over 0–25 °C using a Hot Disk TPS 2500s thermal constants analyzer. Each sample was tested three times, and the
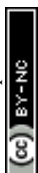
average error was within ±2%.

4.2 Long-term stability and regeneration of NPCEs under flow heat exchange conditions

4.2.1 Experimental setup

Fig. S2 shows the experimental setup, including a heat exchanger, thermostatic water bath, flowmeter, pump, and data acquisition system. The inlet temperatures of both the NPCE and water were controlled by the thermostatic bath. Fluids were circulated through the heat exchanger using a pump, and the inlet and outlet temperatures were monitored using K-type thermocouples. Flow rate and volume were measured by a flowmeter. A 40 mm thick layer of insulating glass wool was used for thermal insulation.

The heat exchanger dimensions were 317 mm × 152.4 mm × 400 mm and consisted of two separate fluid channels [37] to ensure complete cold storage by the NPCE during the heat exchange process.

After 30 and 60 days of operation, the NPCEs were subjected to high-energy regeneration. A high-energy ultrasonic probe was placed into the thermostatic bath, and the NPCEs were regenerated by ultrasonication in three cycles of 10 minutes each at 50% power (500 W), with a 2 s on / 2 s off duty cycle, following the same procedure used for initial emulsification.

4.2.2 Experimental procedures and measurements

The thermal cycling performance of NPCEs over 60 days was tested to simulate their use as cold storage media. During operation, the NPCE tank was maintained at 20 ℃ and the water–ethylene glycol tank at 5 ℃. Both fluids were pumped into the same side of the heat exchanger, where the NPCE underwent full phase change before returning to the thermostatic bath for reheating.

To assess the effect of aging and regeneration, cooling rate tests were conducted for five NPCE states: freshly prepared, after 30 days of cycling, after 30 days with regeneration, after 60 days, and after 60 days with regeneration. In these tests, the heat

exchanger was pre-cooled to 0 °C, and NPCE at 20 °C was pumped through at 100 L h⁻¹. Discharging was considered complete when the temperature difference between inlet and outlet dropped below 3 ℃.

The total cooling energy (E) was calculated from the temperature difference across the exchanger using Eq.(1) [38], assuming negligible heat loss:

$$E = \int_0^t \dot{m} c_p |T_{out} - T_{in}| dt \tag{1}$$

The average cooling power (P) was derived from Eq.(2):

$$P = \frac{E}{t} = \frac{\int_0^t \dot{m} c_p |T_{out} - T_{in}| dt}{t} \tag{2}$$

where $\dot{m}$ is the mass flow rate, c_p the specific heat, t the duration of discharge, and T_{in}, T_{out} the inlet and outlet temperatures.

Author contributions

Yuyao Guo: Writing – original draft, Methodology, Data curation. Jinxin Feng: Data curation, Validation. Zhihao Xia: Investigation, Validation. Ziye Ling: Conceptualization, Formal analysis, Funding acquisition. Xiaoming Fang: Resources, Writing – review & editing. Zhengguo Zhang: Funding acquisition, Supervision.

Conflicts of interest

The authors declare that they have no known competing financial interests or personal relationships that could have appeared to influence the work reported in this paper.

Acknowledgements

Industrial Chemistry & Materials Accepted Manuscript

References

1. K. Pielichowska and K. Pielichowski, Phase change materials for thermal energy storage, *Prog. Mater. Sci.*, 2014, **65**, 67–123.

2. A. A. M. Omara and A. A. A. Abuelnour, Improving the performance of air conditioning systems by using phase change materials: A review, *Int. J. Energy Res.*, 2019, **43**, 5175–5198.

3. J. Feng, J. Huang, Z. Ling, X. Fang and Z. Zhang, Performance enhancement of a photovoltaic module using phase change material nanoemulsion as a novel cooling fluid, *Sol. Energy Mater. Sol. Cells*, 2021, **225**, 111060.

4. J. Feng, Y. Guo, Z. Xia, Z. Ling, X. Fang and Z. Zhang, Performance evaluation and optimization of compact tube-fin latent heat storage system in phase change nanoemulsion discharge mode, *J. Energy Storage*, 2024, **90**, 111893.

5. M. Luo, X. Lin, J. Feng, Z. Ling, Z. Zhang and X. Fang, Fast self-preheating system and energy conversion model for lithium-ion batteries under low-temperature conditions, *J. Power Sources*, 2023, **565**, 232897.

6. J. Zuo, H. Luo, Z. Ling, Z. Zhang, X. Fang and W. Zhang, Preparation of inorganic molten salt composite phase change materials and study on their electrothermal conversion properties, *Ind. Chem. Mater.*, 2024, **2**, 571–586.

7. M. Delgado, A. Lazaro, J. Mazo and B. Zalba, Review on phase change material emulsions and microencapsulated phase change material slurries: Materials, heat transfer studies and applications, *Renew. Sustain. Energy Rev.*, 2012, **16**, 253–273.

8. V. Andersson and J. S. Gudmundsson, Flow properties of hydrate-in-water slurries, *Ann. N. Y. Acad. Sci.*, 2000, **912**, 322–329.

9. Z. Chen and G. Fang, Preparation and heat transfer characteristics of microencapsulated phase change material slurry: A review, *Renew. Sustain. Energy Rev.*, 2011, **15**, 4624–4632.

10. F. Ma and P. Zhang, A review of thermo-fluidic performance and application of shellless phase change slurry: Part 1-Preparations, properties and applications, *Energy*, 2019, **189**, 116246.

11. S. Rashidi, N. Karimi, G. Li and B. Sunden, Progress in phase change nano-emulsions for energy applications-A concise review, *J. Mol. Liq.*, 2023, **387**, 122547.

12. T. Kawanami, K. Togashi, K. Fumoto, S. Hirano, P. Zhang, K. Shirai and S. Hirasawa, Thermophysical properties and thermal characteristics of phase change emulsion for thermal energy storage media, *Energy*, 2016, **117**, 562–568.

13. A. Safari, R. Saidur, F. A. Sulaiman, Y. Xu and J. Dong, A review on supercooling of Phase Change Materials in thermal energy storage systems, *Renew. Sustain. Energy Rev.*, 2017, **70**, 905–919.

14. J. Park, B. Kohn, R. J. Messinger and U. Scheler, Simultaneous effects of thermal cycling and shear on flow instabilities of phase-change nanoemulsions measured by rheo-NMR and MRI velocimetry, *J. Phys. Chem. Lett.*, 2025, **16**, 3316–3325.

15. F. Ran, Y. Chen, R. Cong and G. Fang, Flow and heat transfer characteristics of microencapsulated phase change slurry in thermal energy systems: A review, *Renew. Sustain. Energy Rev.*, 2020, **134**, 110101.

16. H. Niu, W. Wang, Z. Dou, X. Chen, X. Chen, H. Chen and X. Fu, Multiscale combined techniques for evaluating emulsion stability: A critical review, *Adv. Colloid Interface Sci.*,

2023, **311**, 102813.

17. Y. Yu, Y. Chen, S. Mo, J. Chen, Y. Du, L. Jia and Y. Chen, A comprehensive review on preparation, dispersion stability and phase change cycling stability of phase change microemulsions, *Sol. Energy Mater. Sol. Cells*, 2025, **282**, 113426.

18. Z. Applebee and C. Howell, Multi-component liquid-infused systems: A new approach to functional coatings, *Ind. Chem. Mater.*, 2024, **2**, 378–392.

19. S. Ahn, S. Patil and M. Rudolph, Influence of surfactants on selective mechanical separation of fine active materials used in high temperature electrolyzers contributing to circular economy, *Ind. Chem. Mater.*, 2024, **2**, 469–480.

20. Y. Zheng, H. Oguzlu, A. Baldelli, Y. Zhu, M. Song, A. Pratap-Singh and F. Jiang, Sprayable cellulose nanofibrils stabilized phase change material Pickering emulsion for spray coating application, *Carbohydr. Polym.*, 2022, **291**, 119583.

21. F. Wang, C. Zhang, J. Liu, X. Fang and Z. Zhang, Highly stable graphite nanoparticle-dispersed phase change emulsions with little supercooling and high thermal conductivity for cold energy storage, *Appl. Energy*, 2017, **188**, 97–106.

22. S. Barison, D. Cabaleiro, S. Rossi, A. Kovtun, M. Melucci and F. Agresti, Paraffin-graphene oxide hybrid nano emulsions for thermal management systems, *Colloids Surf., A*, 2021, **627**, 127132.

23. S. P. H. Largani, H. Salimi-Kenari, S. R. Nabavi and A. R. Darzi, Manipulation of the thermo-rheological properties of stable Fe_3O_4 nanoparticles-embedded PCM nanoemulsions, *J. Energy Storage*, 2024, **80**, 110351.

24. L. Liu and J. Y. Wu, Developing novel high-performance polyethylene-embedded phase change emulsions with minimal supercooling for efficient thermal energy storage, *Chem. Eng. J.*, 2024, **482**, 148727.

25. L. Liu, J. Niu and J. Y. Wu, Formulation of highly stable PCM nano -emulsions with reduced supercooling for thermal energy storage using surfactant mixtures, *Sol. Energy Mater. Sol. Cells*, 2021, **223**, 110983.

26. L. Liu, J. Niu and J. Y. Wu, Development of highly stable paraffin wax/water phase change material nano-emulsions as potential coolants for thermal management, *Sol. Energy Mater. Sol. Cells*, 2023, **252**, 112184.

27. G. Zhang, Z. Yu, G. Cui, B. Dou, W. Lu and X. Yan, Fabrication of a novel nano phase change material emulsion with low supercooling and enhanced thermal conductivity, *Renew. Energy*, 2020, **151**, 542–550.

28. G. Zhang, Y. Guo, B. Zhang, X. Yan, W. Lu, G. Cui and Y. Du, Preparation and control mechanism of nano-phase change emulsion with high thermal conductivity and low supercooling for thermal energy storage, *Energy Rep.*, 2022, **8**, 8301–8311.

29. D. Cabaleiro, F. Agresti, S. Barison, M. A. Marcos, J. I. Prado, S. Rossi, S. Bobbo and L. Fedele, Development of paraffinic phase change material nanoemulsions for thermal energy storage and transport in low-temperature applications, *Appl. Therm. Eng.*, 2019, **159**, 113868.

30. C. Zhang, J. Ji, X. Zhang and S. Cai, Development of highly stable low supercooling paraffin nano phase change emulsions for thermal management systems, *J. Mol. Liq.*, 2024, **413**, 125905.

31. L. Liu, X. Zhang, H. Liang, J. Niu and J.-Y. Wu, Cooling storage performance of a novel phase change material nano-emulsion for room air-conditioning in a self-designed pilot thermal

storage unit, *Appl. Energy*, 2022, **308**, 118405.

32.   J. Vilasau, C. Solans, M. J. Gomez, J. Dabrio, R. Mujika-Garai and J. Esquena, Stability of oil-in-water paraffin emulsions prepared in a mixed ionic/nonionic surfactant system, *Colloids Surf., A*, 2011, **389**, 222–229.

33.   K. Golemanov, S. Tcholakova, N. D. Denkov and T. Gurkov, Selection of surfactants for stable paraffin-in-water dispersions, undergoing solid-liquid transition of the dispersed particles, *Langmuir*, 2006, **22**, 3560-3569.

34.   E. Günther, T. Schmid, H. Mehling, S. Hiebler and L. Huang, Subcooling in hexadecane emulsions, *Int. J. Refrig.*, 2010, **33**, 1605–1611.

35.   F. Wang, W. Lin, Z. Ling and X. Fang, A comprehensive review on phase change material emulsions: Fabrication, characteristics, and heat transfer performance, *Sol. Energy Mater. Sol. Cells*, 2019, **191**, 218–234.

36.   G. H. Zhang and C. Y. Zhao, Synthesis and characterization of a narrow size distribution nano phase change material emulsion for thermal energy storage, *Sol. Energy*, 2017, **147**, 406–413.

37.   J. Feng, Y. Guo, Z. Ling, X. Fang and Z. Zhang, Performance enhancement and dual-phase change heat transfer mechanism for latent heat storage system using phase change nanoemulsion, *Chem. Eng. Sci.*, 2023, **276**, 118827.

38.   J. Feng, Z. Ling, J. Huang, X. Fang and Z. Zhang, Experimental research and numerical simulation of the thermal performance of a tube-fin cold energy storage unit using water/modified expanded graphite as the phase change material, *Energy Storage Savings*, 2022, **1**, 71–79.

Data availability

The data that supports the findings of this study are available in the ESI of this article.